

THERMO-MECHANICAL MODELING AND THERMAL PERFORMANCE ANALYSIS OF BEAM VACUUM LINE INTERCONNECTIONS AND COLD WARM TRANSITIONS IN HL-LHC LONG STRAIGHT SECTION MAGNETS

J. Harray*, V. Petit, C. Garion, CERN, Geneva, Switzerland

Abstract

The HL-LHC upgrade, aiming at increasing the LHC levelled luminosity by a factor five, relies on novel superconducting magnets requiring a new beam vacuum system. Along with the challenges related to magnet design, the beam optic configuration exposes this new equipment to stringent conditions for vacuum and cryogenic performance. Both cold warm transitions and magnet interconnections appear to be delicate components that are crucial for the thermal heat transfer between diverse subsystems. The proposed study aims at assessing the heat loads to the cryogenic system and the temperature fields in the vacuum system. A nonlinear static thermal analysis is first performed. A thermo-mechanical approach is developed to capture additional thermal resistance arising from contact between components and their behaviour during cool-down. The system is then studied under dynamic operations when beams are circulating and colliding. A thorough analysis of beam-induced heat loads under ultimate conditions highlights the different relevant contributions. Finally, the transient response of the systems is computed to assess thermal time constants.

CONTEXT

High Luminosity

The High Luminosity Large Hadron Collider (HL-LHC) is the ongoing CERN project aiming at multiplying the integrated luminosity of the LHC by a factor 10 [1]. Superconducting insertion magnets in the vicinity of ATLAS (IR1) and CMS (IR5) need to be replaced [2, 3]. Conservative beam-induced heat loads are derived according to the HL-LHC optics v1.5 [4] where the beam operates at $L_0 = 7.5 \cdot 10^{34} \text{ cm}^{-2} \cdot \text{s}^{-1}$ ultimate levelled instantaneous luminosity target and at 7 TeV nominal energy [5].

The study focuses on the thermo-mechanical design of magnet interconnections (IC) and magnet transitions to the ambient referred as cold warm transitions (CWT). Four different CWTs of interest are identified in the experimental insertion area: (i-ii) the two extremities (Q1/D1) of the inner triplet (IT) and (iii-iv) both ends of the stand-alone D2 recombination dipole (IP/NIP). One IC (Q2B/Q3) is investigated and defined as a representative baseline.

Cryogenics and Vacuum

The exposition to highly energetic debris from collision requires the design of shielded beam screens [6, 7]. The

operating temperature of the aperture needs to be in accordance with its required thermodynamic behavior for vacuum integrity [8]. Associated required cooling is of prior interest to draw a rigorous and complete heat budget for the insertion area [9].

Sequence

The analysis studies the system at equilibrium at its cryogenic temperature referred as the stand-by configuration. At this stage, heat transfer mechanisms are either static losses to the ambient or internal exchanges between cryogenic systems. When beam operates, cryogenic regimes are adapted to further extract beam-induced heat loads and reach its ultimate equilibrium. The dynamic transition from stand-by to ultimate configurations is finally assessed.

MODELING

Methods

A multiphysics numerical model is defined in COMSOL Multiphysics®. Thermal conduction equations are derived under a non linear formulation using temperature-dependent properties [10]. Solid mechanics is coupled to heat transfer in one-way. Isotropic and elastic material behavior is considered. Models are meshed in 3D with approximately 250k linear tetrahedron elements. Surface coatings and thin components are modeled under a thin layer approximation with shell elements for computational efficiency.

Mechanical results are computed with a fully coupled direct PARDISO stationary solver. Static thermal results are computed with a direct segregated PARDISO stationary solver. The dynamic behavior is solved with an iterative GMRES transient solver and a time step $\Delta t = 1 \text{ min}$.

Thermal Contact

The joint conductance h_c of contact interfaces is modeled with nonlinear thermo-mechanical contact and the empirical Cooper-Mikic-Yovanovich (CMY) correlation given as [11]:

$$h_c = 1.25k_c \frac{m_{\text{asp}}}{\sigma_{\text{asp}}} \left(\frac{p}{H_c} \right)^{0.94} \quad (1)$$

with p the contact pressure, k_c the harmonic mean of the contacting surface conductivities, σ_{asp} and m_{asp} respectively the RMS value of the average height and slope of surface asperities and H_c the Vickers microhardness of the softer material.

* jerome.harray@cern.ch

The distribution of contact pressure is derived in a one-way coupling from a structural mechanics model. The bolt pretension is applied to the assembly at room temperature. The system is then cooled-down to its cryogenic equilibrium temperature. Temperatures of the interfaces are assumed uniform and postulated a priori in line with the coupling approach. During the cool-down, a loosening of the interface occurs due to the interplay of thermal contractions of the different components. The detrimental decrease of joint conductance is assessed as depicted for D2 in Fig. 1 and thermalization design guidelines are inferred.

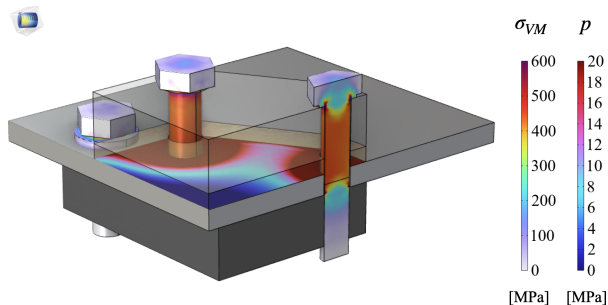


Figure 1: Distribution of contact pressure p at the interface from the thermal shield and von Mises stress σ_{VM} in pretension bolts of D2 NIP.

From the multiphysics approach, a minimum contact pressure from a given tightening torque can be derived for each thermalization design to achieve required heat extraction q as described in Fig. 2 for D2 NIP.

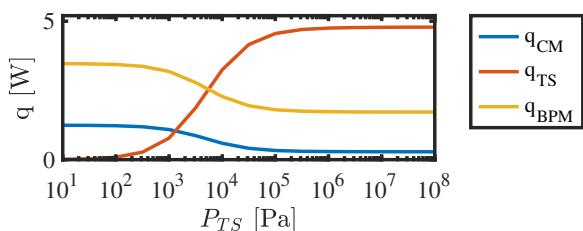


Figure 2: Heat budget of evolution of the cold mass (CM), thermal shield (TS) and beam position monitoring (BPM) according to the average contact pressure P_{TS} of the thermal shield thermalization for D2 NIP.

Internal Isothermal Flow

Natural convection with the ambient is considered on the external surface of the cryostat. Forced convection is modeled for cryogenic circuits. Under isothermal flow assumption with negligible temperature difference between fluid and duct and for ongoing turbulent regimes, heat exchange is computed using Dittus–Boelter correlation [12]:

$$h_f = \frac{k}{D} 0.027 \text{Re}_D^{4/5} \text{Pr}^{1/3} \quad \text{for } \text{Re}_D > 2500, \quad (2)$$

with h_f the internal forced convection coefficient, k the fluid thermal conductivity, ϕ the diameter of the cooling channel, Re_D the dimensionless Reynolds number and Pr the dimensionless Prandtl number.

Surface-to-Surface Radiation

Radiation with the ambient is considered to account for external heat dissipation from CWTs. Regarding surface to surface radiation, the numerical sequence is computationally expensive for large and complex geometries. Its modeling is only implemented when it is relevant to beam line design and the contribution is significant on the overall heat budget. As a first estimate, the radiation from thermal shield to CWT is analytically assessed under the assumption of concentric cylinders [13] and assumed as negligible.

The short length of CWTs, the large aperture D of the beam line and the large temperature difference over CWTs are favorable factors to allow thermal radiation propagating from the ambient to the cold mass through the aperture. This mechanism is referred as beam line radiation in the following and is numerically assessed.

View factors are computed using the hemicube method [14]. Drift tubes and beam screens are truncated over a length L and an enclosure is obtained through virtual capping of the extremities. Black-body properties are assigned to virtual end caps to account for an infinite media. The emissivity of the beam screen is assumed as highly reflective [15]. A minimum length of truncation $L > 5D$ is required to reach representative values of beam line radiation as presented in Fig. 3(a) under a parametric analysis for D2 NIP.

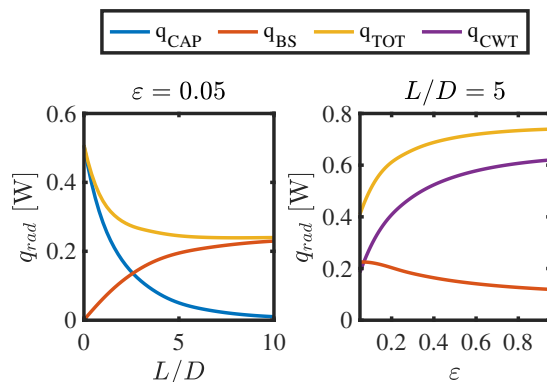


Figure 3: Beam-line radiation budget over the cold mass end cap (CAP), the beam screen surface (BS), their addition (TOT) and the CWT for D2 NIP as a function of (a) the truncation length L and (b) the beam line emissivity ϵ .

The amorphous carbon (a-C) coating from beam screens is known to alter the substrate emissivity but no accurate measurement is made available. Sensitivity analysis is performed to stress involved order of magnitudes and derive conservative radiating heat loads as reported in Fig. 3(b) for D2 NIP.

EXTERNAL CONTRIBUTIONS

During beam operation, interactions with the equipment are leading to power deposition. The contributions of such interactions are referred as beam-induced heat loads. Relevant contributions are reviewed and importation from available dedicated assessments is detailed.

Nuclear Debris

The equipment in the vicinity of collisions is subjected to significant nuclear power deposition. An energy deposition analysis was carried out using FLUKA© [16]. Deposition over D2 is ignored due to distance from collisions. The most significant power deposition from particle showers occurs between Q2A and Q3 and is retained as a conservative case study for IC. Specific power sources are translated into components.

e-Clouds

Simulations of beam-induced electrons multipacting were performed with PyECLOUD onto consecutive 2D sections along the beam line [17, 18]. The secondary electron yield (SEY) of aperture surface is identified as a key parameter. According to ongoing development of a-C coatings [19–21], heat loads are derived considering coated components with SEY = 1.05. Deposition is assumed uniform over aperture sections. A continuous distribution is derived from linear interpolation between studied sections and imposed as a boundary heat load onto beam screen coating.

Impedance

A last beam-induced effect considered is the impedance heating from image current losses. Available studies, computed with CST Studio©, provide linear distributions along beam screens as a function of the copper coating temperature [22]. Results are imported as boundary heat loads and account for two counter-rotating beams in single aperture magnets and the longitudinal weld of the beam screen.

STATIC RESULTS

Temperature

Temperature distributions, as presented in Fig. 4 for Q2B/Q3 IC, are inspected to verify vacuum performance. Temperatures from external surfaces are compared with dew point from ambient conditions to avoid moisture condensation or ice deposition [23].

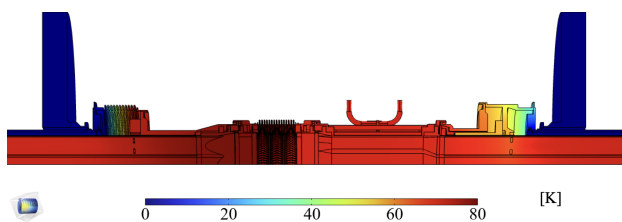


Figure 4: Temperature distribution over Q2B/Q3 IC in stand-by conditions.

Heat Budget

Integrated loads over each cryogenic entities are computed for both stand-by and ultimate conditions and reported to the overall budget for accurate cryogenic design [9]. Beam-induced contributions are identified as the difference between both computed configurations.

MC7: Accelerator Technology

T14: Vacuum Technology

DYNAMIC RESPONSE

Transient responses can be of interest to estimate transit time from stand-by to ultimate equilibrium. The model is initialized from static stand-by configuration computed in previous sections and transient responses are computed with beam-induced heat loads enabled to ultimate values. The minimum, maximum and mean aperture temperatures of the IC are reported in Fig. 5(a) with characteristic times of respectively 0.5 h, 5 h and 4 h. The evolution of the heat extraction from different cryogenic systems is monitored in time as depicted in Fig. 5(b), as an example of the thermalization of the beam position monitoring (BPM) system of the IC with a rising time on the order of 6 h.

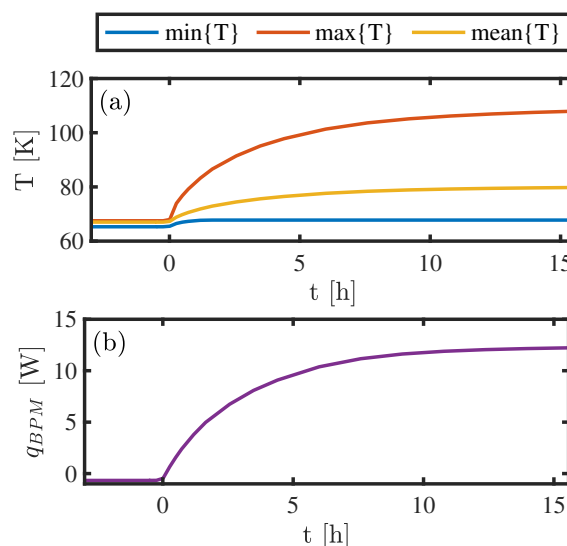


Figure 5: Transient response from stand-by to ultimate conditions for Q2B/Q3 IC of (a) minimum, maximum and mean aperture temperatures and (b) BPM heat flux.

CONCLUSION

Results are comforting for the required vacuum performance. Physics fills generally hold for 10 h to 20 h. Beam line will operate for a significant time below computed conservative ultimate state. Temperature distributions will remain close to the design range leading to desired outgassing rate. Guidelines for thermalization design have been rigorously identified and implemented.

ACKNOWLEDGMENTS

The work is part of the High Luminosity LHC project. The authors wish to acknowledge the colleagues from the groups TE-VSC, SY-STI, TE-CRG and BE-ABP involved in the computations of beam-induced heat loads. The authors personally acknowledge M. Sabate Gilarte (SY-STI) for the dedicated post-processing of energy deposition results; V. Gahier and P. Zijm (TE-CRG) for the discussions around computed values and the overall heat budget; and the Swiss COMSOL office for the genuine support and the fruitful collaboration around implemented numerical methods.

THPOTK035

2841

REFERENCES

- [1] G. Apollinari, O. Bruening, T. Nakamoto, and L. Rossi, "High Luminosity Large Hadron Collider HL-LHC," 2015, arXiv:1705.08830 [physics]. doi: 10.5170/CERN-2015-005.1.
- [2] E. Todesco *et al.*, "A first baseline for the magnets in the high luminosity Lhc insertion regions," *IEEE Transactions on Applied Superconductivity*, vol. 24, no. 3, pp. 1–5, 2014. doi: 10.1109/TASC.2013.2288603.
- [3] E. Todesco *et al.*, "Superconducting magnet technology for the upgrade," in *The High Luminosity Large Hadron Collider: The New Machine for Illuminating the Mysteries of Universe*, World Scientific, 2015, pp. 107–135. doi: 10.1142/9789814675475_0006.
- [4] J. D. Andersson, D. Gamba, and R. De Maria, "Orbit correction studies on the HL–LHC layout and optics v1.5," Tech. Rep. CERN-ACC-NOTE-2020-0045, 2020.
- [5] E. Métral *et al.*, "Update of the HL-LHC operational scenarios for proton operation," Tech. Rep. CERN-ACC-NOTE-2018-0002, 2018.
- [6] C. Garion, V. Baglin, and R. Kersevan, "Preliminary design of the high-luminosity LHC beam screen with shielding," in *Proc. IPAC'15*, (Richmond, VA, USA, May 2015), 2015, pp. 60–63. doi: 10.18429/JACoW-IPAC2015-MOBD1.
- [7] C. Garion, L. Dufay-Chanat, T. Koettig, W. Machiocha, and M. Morrone, "Material characterisation and preliminary mechanical design for the HL-LHC shielded beam screens operating at cryogenic temperatures.," *IOP Conference Series: Materials Science and Engineering*, vol. 102, p. 012013, 2015. doi: 10.1088/1757-899X/102/1/012013.
- [8] R. Kersevan, "Synchrotron radiation distribution and related outgassing and pressure profiles for the HL-LHC final focus magnets," in *Proc. IPAC'15*, (Richmond, VA, USA, May 2015), pp. 3127–3130. doi: 10.18429/JACoW-IPAC2015-WEPHA012.
- [9] S. Claudet *et al.*, "Cryogenics for the HL-LHC," in *High-Luminosity Large Hadron Collider (HL-LHC): Preliminary Design Report*, 2020, ch. 9. doi: 10.48550/arXiv.1705.11078.
- [10] E. Marquardt, J. Le, and R. Radebaugh, "Cryogenic material properties database," in *Cryocoolers 11*, Springer, 2002, pp. 681–687.
- [11] M. Cooper, B. Mikic, and M. Yovanovich, "Thermal contact conductance," *International Journal of Heat and Mass Transfer*, vol. 12, no. 3, pp. 279–300, 1969.
- [12] F. W. Dittus and L. M. K. Boelter, "Heat transfer in automobile radiators of the tubular type," *University of California Publications in Engineering*, vol. 2, pp. 443–461, 1930.
- [13] R. Greif and G. P. Clapper, "Radiant heat transfer between concentric cylinders," *Applied Scientific Research*, vol. 15, no. 1, pp. 469–474, 1965, issn: 0003-6994, 1573-1987. doi: 10.1007/BF00411578.
- [14] M. F. Cohen and D. P. Greenberg, "The hemi-cube: A radiosity solution for complex environments," ser. SIGGRAPH '85, New York, NY, USA: Association for Computing Machinery, 1985, pp. 31–40, isbn: 0897911660. doi: 10.1145/325334.325171.
- [15] J. Frolec, T. Králík, V. Musilová, P. Hanzelka, A. Srnka, and J. Jelínek, "A database of metallic materials emissivities and absorptivities for cryogenics," *Cryogenics*, vol. 97, pp. 85–99, 2019, issn: 0011-2275. doi: https://doi.org/10.1016/j.cryogenics.2018.12.003.
- [16] M. Sabaté-Gilarte and F. Cerutti, "Energy deposition study of the CERN HL-LHC optics v1.5 in the ATLAS and CMS insertions," in *Proc. IPAC'21*, (Campinas, Brazil, May 2021), pp. 76–79. doi: 10.18429/JACoW-IPAC2021-MOPAB012.
- [17] G. Skripka and G. Iadarola, "Electron cloud build-up in two-beam regions for HL-LHC, heat load and vacuum aspects," *CERN Yellow Reports: Conference Proceedings*, vol. 7, pp. 59–59, 2020. doi: 10.23732/CYRCP-2020-007.59.
- [18] G. Skripka and G. Iadarola, "Beam-induced heat loads on the beam screens of the inner triplets for the HL-LHC," Tech. Rep. CERN-ACC-NOTE-2018-0009, 2018. doi: 10.17181/CERN.I7WJ.TNS9.
- [19] R. Salemme, V. Baglin, G. Bregliozzi, P. Chiggiato, and R. Kersevan, "Amorphous carbon coatings at cryogenic temperatures with LHC type beams: First results with the COLDEX experiment," in *Proc. IPAC'15*, (Richmond, VA, USA, May 2015), pp. 3112–3114. doi: 10.18429/JACoW-IPAC2015-WEPHA007.
- [20] C. Y. Vallgren *et al.*, "Amorphous carbon coatings for mitigation of electron cloud in the CERN SPS," in *Proc. IPAC'10*, (Kyoto, Japan, May 2010), pp. 2033–2035. doi: 10.1103/PhysRevSTAB.14.071001.
- [21] M. V. Gompel *et al.*, "Amorphous carbon thin film coating of the SPS beamline: Evaluation of the first coating implementation," in *Proc. IPAC'17*, (Copenhagen, Denmark, May 2017), pp. 44–47. doi: 10.18429/JACoW-IPAC2017-MOCCA3.
- [22] E. Métral and C. Zannini, "Temperature effects on image current losses in the HL-LHC triplets—part 2," in *33rd HiLumi WP2 Task Leaders Meeting, CERN*, vol. 5, 2014.
- [23] M. G. Lawrence, "The relationship between relative humidity and the dewpoint temperature in moist air: A simple conversion and applications," *Bulletin of the American Meteorological Society*, vol. 86, no. 2, pp. 225–234, 2005. doi: 10.1175/BAMS-86-2-225.